Design of a nitrogen-implanted titanium-based superelastic alloy with optimized properties for biomedical applications

D.M. Gordin, Denis Busardo, A. Cimpean, C. Vasilescu, Daniel Höche, S.I. Drob, V. Mitran, Maryline Cornen, Thierry Gloriant

Design of a nitrogen-implanted titanium-based superelastic alloy with optimized properties for biomedical applications

D.M. Gordin[1], D. Busardo[2], A. Cimpean[3], C. Vasilescu[4], D. Höche[5], S. I. Drob[4], V. Mitran[3], M. Cornen[1], T. Gloriant[1*]

[1]*INSA de Rennes, Laboratoire Chimie-Métallurgie, UMR CNRS 6226 Institut des Sciences Chimiques de Rennes, 20 avenue des Buttes de Coësmes, 35708 Rennes Cedex 7, France*

[2]*Quertech Ingénierie, 9 rue de la Girafe, 14000 Caen, France*

[3]*University of Bucharest, Department of Biochemistry and Molecular Biology, Spl. Independentei 91-95, 050095, Bucharest, Romania*

[4]*Institute of Physical Chemistry «Ilie Murgulescu» of Romanian Academy, Spl. Independentei 202, 060021, Bucharest, Romania*

[5]*Institute of Materials Research, Helmholtz-Zentrum Geesthacht -Zentrum für Material- und Küstenforschung GmbH Max-Planck-Straße 1, D-21502 Geesthacht, Germany*

**Corresponding author: Prof. Thierry Gloriant*
Tel/Fax : +33.(0)2.2323.8241/8240
email : Thierry.Gloriant@insa-rennes.fr

Abstract

In this study, a superelastic Ni-free Ti-based biomedical alloy was treated in surface by implantation of nitrogen ions for the first time. The N-implanted surface was characterized by X-ray diffraction, X-ray photoelectron spectroscopy, secondary ion mass spectroscopy, and the superficial mechanical properties were evaluated by nano-indentation and by ball-on-disk tribological tests. To investigate the biocompatibility, the corrosion resistance of the N-implanted Ti alloy was evaluated in simulated body fluids (SBF) complemented by *in-vitro* cytocompatibility tests on human fetal osteoblasts. After implantation, surface analysis methods revealed the formation of a titanium-based nitride on the substrate surface. Consequently, an increase in superficial hardness and a significant reduction of friction coefficient were observed compared to the non-implanted sample. Also, a better corrosion resistance and a significant decrease in ion release rates have been obtained. Cell culture experiments indicated that the cytocompatibility of the N-implanted Ti alloy was superior to that of the corresponding non treated sample. Thus, this new functional N-implanted titanium-based superelastic alloy presents the optimized properties that are required for various medical devices: superelasticity, high superficial mechanical properties, high corrosion resistance and excellent cytocompatibility.

Keywords: titanium alloy, ion implantation, surface analysis, corrosion resistance, biocompatibility

1. Introduction

During the last years, intense research was performed in order to develop highly biocompatible titanium-based alloys for medical applications [1-8]. Metastable beta titanium alloys were shown to be excellent candidates, due to the possibility to elaborate them only with fully biocompatible elements such as Ta, Nb, Mo, Zr [7-9]. A metastable beta titanium alloy can be obtained if a sufficient amount of β-stabilizing elements is added to retain at room temperature the β microstructure (body centered cubic) after quenching from the beta domain. It is shown in the literature that the microstructure and the mechanical properties of metastable β titanium alloys are very sensitive to composition changes and thermal treatments [6,10,11]. In a given composition domain, the metastable β microstructure may be mechanically unstable. Then, the quenched β microstructure is decomposed into a stress-induced α" martensite (C-centered orthorhombic) when an external stress is applied. This phenomenon is generally highlighted by a characteristic tensile stress-strain curve showing a nonlinear elastic domain and a stress plateau associated with a double yielding behavior. As the stress-induced martensitic transformation is reversible, a high recoverable strain can be obtained, leading to a superelastic effect [4,6,8]. Thus, these non-allergen Ni-free alloys can be envisaged to replace the superelastic NiTi-based materials currently used for the fabrication of functional biomedical dispositive such as arches, wires and other springs used in orthodontics, endodontic instruments, cardiovascular or pulmonary stents, wires and catheters for the cardiovascular surgery, staples and prostheses of articulations for the orthopedic surgery [7,8]. On the other hand, the superelastic effect is accompanied by a very significant reduction of the elastic modulus, which is very beneficial for the use of these alloys like prostheses or implants in osseous site (articulations prostheses, dental implants). Indeed, a low elastic modulus reduces the stress-shielding effect that is caused by a difference in the elastic modulus of the bone substitute and the natural human bone that affects long-term performances in service [12,13].

Nevertheless, the main weaknesses of titanium alloys are their poor friction and wear resistance. Specifically, in the case of head prostheses, their surface has to be treated or re-enforced in order to better resist friction and to reduce wear particles release [14,18].

. On the other hand, metallic materials implanted in human body, must have a high corrosion resistance to avoid the release of ions and corrosion products in the surrounding tissues that can ultimately affect their biocompatibility [19-25]. A well-known and reliable

surface treatment process that can enhance both surface mechanical properties and corrosion resistance of titanium alloys can be ion implantation [26-28]. As concerns nitrogen implantation, besides the increased surface hardness and wear resistance, this surface modification procedure was associated with improved corrosion resistance [28]. In addition, several *in vitro* and *in vivo* studies demonstrated the superior biological performance of nitrogen-implanted titanium based materials [29-31]. It is worth noting that most of the studies found in literature dealing with the ion implantation of biomedical titanium alloys concern the Ti-6Al-4V and CP-Ti alloys commonly used in medicine and, to our knowledge, no study mentions ion implantation on metastable β Ti-based superelastic alloys.

The aim of the study is then to investigate the superficial characteristic changes of a superelastic Ti-based alloy after implantation of nitrogen ions in surface. As superelastic alloy, the Ti-25Ta-25Nb alloy composition was chosen because a complete investigation of its microstructure and its superelastic behaviour was carried out in previous studies [32,33]. On the other hand, an original ion implantation technique developed and patented by *Quertech Ingénierie* Company (France) was used. In this work, the microstructural changes and the mechanical property modifications in surface were investigated by Grazing Incidence X-ray Diffraction (GIXRD), X-ray Photoelectron Spectroscopy (XPS), Secondary Ion Mass Spectroscopy (SIMS), nano-indentation and ball-on-disk tribological tests after nitrogen implantation. As the N-implanted Ti-25Ta-25Nb superelastic alloy is of great interest for biomedical applications, its corrosion behaviour in simulated body fluid (SBF) and its biocompatibility using *in vitro* tests performed on human fetal osteoblasts were also evaluated in the present study.

2. Materials and methods

2.1. Alloy preparation and implantation method

The Ti-25Ta-25Nb alloy composition (25 mass. % of Ta, 25 mass. % of Nb and the balance mass. % of Ti) was synthesized by cold crucible levitation melting technique (CCLM) under high vacuum. For the synthesis, pure raw metals were used (purities: 99% for Ti and 99.9% for Ta and Nb). Ingots, presenting a near pancake shape after melting, were next homogenized at 1223K for $72x10^3$s under high vacuum, followed by water quenching.

Ingots of about 10mm in thickness were then cold rolled at room temperature ~~until a~~ by approximately 90% of reduction to reach 1mm in thickness. From this cold-rolled state, samples were cut in square pieces (1mm x 20mm x 20mm), then solution-treated in the β-phase domain at 1123K for $1.8x10^3$s under vacuum in order to restore a fully recrystallized microstructure and finally water quenched to retain the metastable β microstructure at room temperature. As previously mentioned in the introduction, an investigation of the microstructure and the tensile properties of the metastable beta Ti-25Ta-25Nb alloy synthesised by this process was carried out in a previous work [33]. In Fig. 1, it is reported the typical tensile curve exhibiting a double yielding behavior characteristic of the superelastic property that possesses such alloy. From this curve a low incipient Young's modulus measured at 55 GPa was found, which is very low compared to that obtained from classical titanium alloys currently used in medicine (110 GPa) and closer to the one that corresponds to the cortical bone (20-30 GPa).

Before ion implantation, square samples were first mechanically polished on silicon carbide abrasive papers (up to 4000 grit) followed by a final polishing step with a colloidal silica suspension (particles size: 50 nm) and then ultrasonically cleaned in acetone, thoroughly washed with ethanol and dried in air. In this work, an original ion implantation technique developed and patented by *Quertech Ingénierie* was used. This process (trademark *Hardion+*) is based on the use of an Electron Cyclotron Resonance (ECR) ion source to produce a multienergetic ion beam from multicharged ions (N^+, N^{2+}, N^{3+}…). The N^{i+} ions have energy and a depth of implantation in time higher than the N^+ ion. Consequently, these multicharged ions are implanted simultaneously at various depths giving a profile of concentration relatively flat and deeper by comparison with the conventional monoenergetic ion implantation technique [34]. The great advantage of this technology is that the ion implantation was carried out in a micro-implanter (30 cm for 10 kg) using permanent magnets mainly composed of the ECR ion source coupled to a vacuum chamber. Currently, the *Hardion+* technology can treat only flat surfaces but the use of such micro-implanter technology must make it possible to overcome the geometry limitation imposed by traditional linear ion implantation.

Using this technology, nitrogen ions (N^+ to N^{5+}) were implanted with the same dose ($5x10^{17}$ ions.cm^{-2}) in all samples with an average energy of 100 keV (ion beam intensity of 4 mA). During the implantation, the titanium alloy sample is placed on a water cooled holder

which moves under the ion beam. Taking into account the speed used (40 mm.s^{-1}), the surface temperature was always measured to be lower than 50°C.

In order to carry out all the experiments and characterizations and to obtain a correct statistical evaluation, more than 100 samples were implanted in this study.

2.2 Surface characterization methods

Phase identification of the N-implanted surface was carried by Grazing Incidence X-ray Diffraction technique (GIXRD) using a Bruker D8 Discover diffractometer working at 40 kV with the Cu Kα radiation in a glancing geometry (incidence angle fixed at 1°). On the other hand, an analytical study using X-ray Induced Photoelectron Spectroscopy (XPS) has been carried out on a Kratos Axis Ultra DLD working with a 15 kV X-ray gun and monochromatic AlK_{α} radiation. The analysed area size was 700 x 300 microns and the pass energy was set to 20 eV during region scans (energy resolution of 0.1 eV). Additionally, argon ions at 4 keV have been used to etch for 1800 s (2 mm²) in order to obtain a depth profile. By deconvolution of the binding energies on Ti 2p, N 1s, Nb 3d and Ta 4d core levels, the present chemical bonds have been studied in detail.

Secondary ion mass spectroscopy (SIMS) experiments were carried out on a Hiden analytical system including the IG20 ion gun using Ar+ ions at 5 keV and a MAXIM-Quadrupole mass detector. The focused beam has a diameter of 100 µm at about 500 nA beam current. To avoid edge effects at the crater, the beam was rasterised across the sample (0.65 x 0.45 mm). Signals were just measured in the inner gate of approximately 0.15 x 0.1 mm.

Superficial mechanical properties were studied by nano-indentation with a CSM NHT instrument equipped with a diamond Berkovich-type indenter. For the measurements, the continuous stiffness mode was used. Thus, indentations were made perpendicularly to the sample surface using the oscillating mode with 2 mN increasing step that allowed hardness-depth profile plot. 10 measurements were made to plot the average hardness profile, before and after ion implantation.

Ball-on-disk tribological tests were performed with a CSM tribometer to evaluate friction coefficient and wear resistance of treated surfaces. Friction coefficient was monitored during sample surface sliding against an alumina ball (6 mm diameter) in ambient atmosphere. The applied load and sliding velocity were 0.25 N and 0.01 m s^{-1}, respectively.

2.3. Corrosion behaviour testing

The surfaces of non-treated and N-implanted Ti-25Ta-25Nb specimens with an area of 1 cm^2 were degreased in acetone, washed with bi-distilled water and dried in air. Their electrochemical behaviour in simulated body fluids (SBF) of different pH values (3.08; 7.21; 9.07) was studied. Different pH values were selected to simulate the severe functional conditions of an implant: in case of surgery, the hydrogen concentration increases in the traumatized tissues till pH of 3 – 5 values [35]; the ulterior infections or inflammations can produce the increase of pH values till 9 [36,37].

SBF composition was (g l^{-1}): NaCl – 6.0; KCl – 0.4; $CaCl_2$ – 0.2; sodium lactate – 3.05; pH = 7.21 was its normal pH; pH = 3.08 was obtained by HCl addition; pH = 9.07 was obtained by KOH addition.

The corrosion behaviour of the N-implanted and non-treated Ti-25Ta-25Nb alloy was appreciated from the cyclic polarization curves, linear polarization (Tafel representation) and monitoring of the open circuit potentials and corresponding open circuit potential gradients.
The cyclic potentiodynamic polarization was applied starting from about -0.8 V to +2.0 V (vs. SCE) with a scan rate of 1 mV s^{-1}. Voltalab 80 equipment with its VoltaMaster 4 program was used. From voltammograms, the main electrochemical parameters were determined [38]: E_{corr} - corrosion potential, like zero current potential, E_p – passivation potential at which the current density is constant; $|E_{corr} - E_p|$ difference represents the tendency to passivation (low values characterize a good, easy passivation); ΔE_p – passive potential range of the constant current; i_p – passive current density.

The linear polarization method was used to obtain the polarization resistance, R_p, the corrosion current densities, i_{corr}, corrosion, V_{corr} and the ion release rates. The linear polarization was performed for ±50 mV around the open circuit potential at a scan rate of 0.1 mV s^{-1} using the same Voltalab 80 equipment. VoltaMaster 4 program directly supplies the values of R_p, i_{corr} and V_{corr}. Ion release rates (ng cm^{-2}) were calculated [38]:

$$\text{Ion release} = 1.016\ V_{corr}\ 10^5 \quad (1)$$

where V_{corr} = corrosion rate in μm y^{-1}.

Open circuit potentials E_{oc} were monitored (for 2000 immersion hours in physiological solutions) using Hewlett-Packard multi-meter. In the long-term functional

conditions of an implant, the pH non-uniformities of the human biofluid can appear in the distress periods (till 9 value) [37] or due to the hydrolysis of the corrosion products (till 2-3 value) [38]; so, different zones of an implant can be in contact with physiological fluid of various pH values which can generate different values of the open circuit potentials; thus, differences of the open circuit potentials ΔE_{oc} can form on the implant surface; these potential differences can initiate galvanic corrosion that can accelerate the implant corrosion process; consequently, the following open circuit potential differences which can appear due to the pH non-uniformities $\Delta E_{oc}(pH)$ along the alloy surface were determined:

$$\Delta E_{oc1}(pH) = E_{oc}^{pH=3.08} - E_{oc}^{pH=7.21} \quad (2)$$

$$\Delta E_{oc2}(pH) = E_{oc}^{pH=3.08} - E_{oc}^{pH=9.07} \quad (3)$$

$$\Delta E_{oc3}(pH) = E_{oc}^{pH=7.21} - E_{oc}^{pH=9.07} \quad (4)$$

2.4. In vitro assessment of osteoblast behaviour

2.4.1. Cell culture

The cell culture study was conducted with the American Type Culture Collection CRL-11372™ (hFOB 1.19) human-foetal-osteoblasts, a human pre-osteoblastic cell line. This cell line is transfected with a gene that codes for the temperature sensitive mutant (tsA58) of the SV 40 T-antigen, together with a gene coding for gentamycin resistance [39]. For performing any kind of biological experiments, three samples of each type (N-implanted and non-treated Ti-25Ta-25Nb) were sterilized at 180°C for 30 min and placed individually into the wells of the 6-well (for test samples of 25x25x1 mm in the MTT and LDH assays) and 12-well (for test samples of 10x10x1 mm in the microscopy study) Multiwell culture plates. Surfaces were seeded with cells at an initial density of 10^4 cells·cm^{-2} and incubated at a temperature of 34°C in a humidified incubator containing 5% CO_2. Pre-osteoblastic cells hFOB 1.19 were maintained in Dulbecco's Modified Eagle's Medium/ Ham's Nutrient Mixture F-12 [DMEM/F12-1:1 (w/w) mix] containing 10% (v/v) fetal bovine serum (FBS) and 0.3 mg·mL^{-1} neomycin (G418) for specific times. The medium was changed every third day up to 7 days excepting the cytotoxicity assay when the culture medium was replaced in the second and fourth day of culture.

2.4.2. Cytotoxicity assay

The effect of non-treated and N-implanted Ti-25Ta-25Nb samples on cell viability was assessed using lactate dehydrogenase (LDH) release assay. This study was performed by using a cytotoxicity detection kit (TOX-7, Sigma-Aldrich Co.) according to the manufacturer's protocol. High OD_{490nm} values are indicatives of a reduction in the cell viability

2.4.3. Fluorescence staining of the actin and fibronectin

Cell attachment, spreading and morphology were assessed by fluorescent staining of actin cytoskeleton at 1 h, 4 h and 24 h post seeding. Briefly, at the end of the incubation period, cells were washed with phosphate buffer saline (PBS) three times and fixed with 4% paraformaldehyde for 20 min. Fixed cells were rinsed with PBS and permeabilized for 1 h with 0.1% Triton X-100/2% BSA followed by three 10-min PBS washes. Afterwards, the permeabilized cells were incubated with phalloidin-TRITC (tetramethylrhodamine B isothiocyanate) (20 $\mu g \cdot mL^{-1}$; Sigma-Aldrich Co.) for 1 h at 37^0C to label actin filaments. The nuclei were stained for 15 min with DAPI (4',6-diamidino-2-phenylindole) at a concentration of 2 $\mu g \cdot mL^{-1}$ in PBS. For immunolocalization of the extracellular matrix (ECM) protein, fibronectin (FN), fixed and permeabilized samples were processed as previously shown [40]. In both studies, images from representative fields of each sample were viewed with an inverted fluorescent microscope Olympus IX71 and captured by means of Cell F image acquiring system.

2.4.4. Cell proliferation assay

To evaluate cell proliferation potential, the cells on days 2, 4 and 7 after seeding on non-treated and N-implanted Ti-25Ta-25Nb surfaces were incubated with 0.5 $mg \cdot mL^{-1}$ MTT [3-(4, 5-dimethyl thiazol-2-yl) 2, 5-diphenyltetrazolium bromide] solution according to tetrazolium-based colorimetric assay described by Mosman [41]. The mitochondrial enzyme succinate-dehydrogenase within viable cells is able to reduce the yellow dye MTT to a purple colored product (formazan) which is soluble in dimethyl sulfoxide (DMSO). The amount of formazan produced, whose absorbance was recorded at 550 nm with the Thermo Scientific Appliskan microplate reader, was proportional to the number of viable, metabolically active cells present.

2.4.5. Statistical analysis

For the statistical analysis of the LDH and MTT assays, one-way ANOVA with Bonferroni's multiple comparison tests was performed. All values are expressed as mean value±standard deviation of three independent experiments and differences at $p \leq 0.05$ were considered statistically significant.

3. Results and discussion

3.1. Surface characterization

GIXRD patterns from the Ti-25Ta-25Nb alloy are presented in Fig. 2. For the non-treated surface, the diffracted peaks are related to the β phase (body centered cubic) which constitutes the microstructure of the bulk alloy. After nitrogen implantation, additional peaks are observed and can be clearly attributed to a face centred cubic nitride phase formation (space group: Fm-3m) such as TiN, TaN or NbN. Although the XRD pattern in Fig. 2 was indexed with the TiN phase, the nitride obtained is not only composed with Ti an N atoms. Indeed, the cell parameter, evaluated to be 0.4266 nm in the present study, is higher than the one obtained from pure TiN (0.4238 nm according the 1-71-299 JCPDS card n°). Consequently, Ta and Nb elements can partially substitute Ti in the nitride solid solution.

To determine the chemical states, high resoluted XPS spectra have been measured at the N 1s, Ti 2p, Nb 3d and Ta 4d core levels as shown in Fig. 3. The binding energy of the N 1s state was measured to be between 397.0 eV and 397.3 eV according to the convolution of three signals from TiN (literature 397.2 eV [42]), TaN (397.0 eV [43]) and NbN (397.3 eV [44]) bonds. Thus, it is confirmed all nitrogen atoms are in chemical bond to titanium, to tantalum and niobium, excepting the surface contaminations with hydrocarbon. The Ti $2p_{3/2}$ signal at 455.2 eV is contributed to the Ti-N bond [42] (metallic bulk core level 454.1 [45,46]). Ti-O bonds around 459 eV [47] are predominantly very close to the surface due to the contamination effects. Nb-N signals occurred at 203.6 (literature 203.8 [48]) whereas the metallic peak was measured at 202.2 eV (literature 202.4 eV [48]). A weak oxide peak at 207.2 eV (207.4 eV [48]) on the very surface occurred as well (artifical argon signals around 242 eV are related to the etching). In relation to niobium, the tantalum pentaoxide peak is much stronger at 229.9 eV (230.1 eV [49]). In depth the nitride formation looks very similar to Nb and Ti. The peaks occurred at 228.0 eV for the nitride and 226.3 eV (226.4 eV [50]) for

the metallic state. Close to the surface contamination effects become visible for all studied excitation states. Beside classical hydrocarbon the affinity of oxide formation has been shown for all alloying elements. All peaks have been deconvoluted by means of Gauss-Lorentz GL (30) peak functions and Shirley backgrounds with respect to the orbit split of the 2p1/2 and 2p3/2 state having an area ratio of 1:2, respectively the 3d/4$d_{3/2}$ and 3d/4$d_{5/2}$ orbital split with an area ration 2:3. Thus, Ti 2$p_{1/2}$, Nb 3$d_{3/2}$ and Ta 4$d_{3/2}$ have not been discussed separately.

SIMS depth profiles were shown in Fig. 4. They verify the observed elemental distribution by XPS. Especially, the TaN^-, TiN^- -and NbN^- ion distributions are very similar. Curve shape development is shown by sketching the multi ion distribution for the TaN^- depth profile. The varying count rates are related to different sputter and detection efficiencies arising from different atomic weight and size (Ti<Nb<Ta). This behaviour can also be observed on the bare Nb^- and Ta^- profile since the count rates are higher for nitrides compared to the bulk matrix. The shape of the depth profiles describes and follows the multi ion implantation process and at least in the arising sputter efficiency.

*3.2 Nano-indentation and friction measurement*s

Mean hardness vs. tip penetration depth profiles of N-implanted and non-implanted samples are shown in Fig. 5. From the N-implanted sample, the nano-indentation profile begins at a high hardness value and then decreases until reaching the non affected zone in the core of the alloy. One can notice that the non-implanted sample profile also presents that trend to a lesser extent. This can be attributed to work hardening due to mechanical polishing. In Fig. 5, a hardness increasing in the first 600 nm due to nitrogen implantation is clearly evidenced. A maximum hardness value at about 8.5 GPa is then obtained after N-implantation, which corresponds to an increasing of almost twice the hardness value of the bulk alloy.

Fig. 6 presents typical evolutions of friction coefficients as function of the number of cycles for N-implanted and non-implanted samples during ball-on-disk tribological tests. It is clearly showed that the N-implanted sample possesses a reduced friction coefficient by comparison with the non-treated sample. After an accommodation period, the friction coefficient of the N-implanted sample is stabilized at about 0.3, which corresponds to a significant reduction of around a factor 2.7 by comparison with the non-implanted sample. In Fig. 6, it is also presented optical micrographs showing the wear tracks obtained after 200 cycles of friction. It can be clearly observed that the N-implanted sample has a narrow wear

track compared to the non-treated one. The measurements indicate a wear track thickness reduction of about 85% under the experimental conditions used: 200 cycles under 0.25N load.

These increased hardness and wear resistance are clearly due to the nitride formation on surface, which was detected by GIXRD, XPS and SIMS. In addition, hardness profile measurements are in good agreement with the XPS profile. Indeed, both methods show that the affected depth is about 600 nm after nitrogen implantation.

3.3. Corrosion behaviour

From cyclic potentiodynamic curves (Fig. 7) it can be observed that both non-treated and N-implanted Ti-25Ta-25Nb alloys exhibited passive behaviour in all studied biofluids. The N-implanted alloy had a nobler electrochemical behaviour than the non-treated sample, proved by the more favourable electrochemical parameters (Table 1): more electropositive corrosion (E_{corr}) and passivation (E_p) potentials, lower tendencies to passivation $|E_{corr} - E_p|$, i.e. an easier passivation, and lower passive current densities i_p, showing a more resistant passive layer. These facts can be explained only by the presence of the nitrided layer that acts as a barrier layer against the metallic ion transport through it, into aggressive solutions. The most favourable electrochemical parameters for N-implanted alloy were registered in neutral (pH = 7.21) SBF, the normal functional conditions of an implant; these parameters revealed a very good passive behaviour. In severe functional conditions, simulated by the acid (pH = 3.08) and alkaline (pH = 9.07) SBF, the main electrochemical parameters for N-implanted Ti-25Ta-25Nb presented better values than the non-treated alloy, indicating a very good passive behaviour. Passive current densities i_p for N-implanted alloy represented about a half from the passive current densities of the non-treated alloy as result of the better protection, conferred by the implantation layer.

Corrosion current densities i_{corr} and corresponding corrosion V_{corr} and ion release rates (obtained from linear polarization measurements) of the N-implanted alloy (Table 2) are lower than those of the non-treated one and are placed in the "Perfect Stable" resistance class [36], proving the protective properties of the nitride layer. The polarisation resistances R_p are higher for the N-implanted alloy than for non-treated one, demonstrating a more protective, more resistant layer that reduced the ion release rate and corresponding alloy toxicity. The lowest corrosion and ion release rates were obtained in neutral SBF, condition in which an implant "works" the most time from its "service life". Taking into account that the N-

implanted alloy presented better anticorrosive resistance, it results that the implantation layer is very effective both in normal and severe functional conditions.

Monitoring of the open circuit potentials for 2000 immersion hours in the studied simulated biofluids (Fig. 8) showed that these potentials for the N-implanted alloy are more electropositive than those of non-treated alloy that means a more resistant layer; the open circuit potentials tended to nobler values in time and reached a constant level at about 1000 immersion hours that indicate the improvement of the protective state [51,52]. In acid and alkaline SBF, the slight more electronegative open circuit potentials than in neutral SBF were observed due to the higher aggression of these solutions; nevertheless, their values are placed in the noble potential range (about -100 mV), revealing a passive resistant state.

Open circuit potential gradients (Table 3) had low values that cannot generate galvanic cells, because only differences of 0.6 – 0.7 V (in absolute value) [53,54] can initiate and maintain this type of corrosion. It can be concluded that the galvanic corrosion cannot develop on the implant surface even in the severe case of a very large pH difference between acid (3.08) and alkaline (9.07) pH values (ΔE_{oc2}).

3.4. In vitro biological response

Cell culture models are routinely used to gain insight into the bone-cell response to candidate orthopedic biomaterials *in vitro*. In order to evaluate the effect of nitrogen implantation by Hardion+ micro-implanter technology on the biocompatibility of the recently developed and characterized beta-type titanium alloy, Ti-25Ta-25Nb [55], we first studied the LDH release in the culture medium at different periods of time. This procedure gave us information about the cytotoxicity of the analyzed materials as represents an indicator of cell membrane integrity. As shown in Fig. 9, hFOB 1.19 cells grown on non-treated and N-implanted Ti-25Ta-25Nb samples proved to display low LDH release in culture medium without statistically significant differences ($p>0.5$) between the two groups. These results indicate that nitrogen implantation has no direct effect on the release of LDH and does not exert cytotoxic effects. This finding is also supported by the morphological features of the osteoblasts noticed by fluorescence microscopy (Fig. 10) of the cells labeled with phalloidin-TRITC at 1 h, 4 h and 48 h after cell plating. It can be seen that, at 4 h post-seeding, on both surfaces the initial round cells rapidly assumed the elongated, spindle-shaped appearance typical of osteoblast-like cells plated onto TCPS. Cortical actin bundles predominantly appeared at the peripheries of cells, consistent with a less-spreading and rounded up

morphology [56]. The cells attained a well spread morphology characterized by significantly higher cell area, more evident on N-implanted surface, at 48 h after culture initiation. They displayed prominent actin stress fibers that appeared to be arranged parallel to the long axis of the cell. Taking into account that there is a close relationship between stress fiber formation and cell adhesion [57], this finding suggests that nitrided Ti-25Ta-25Nb surfaces favour bone cell adhesion.

This last observation is in agreement with the MTT reduction assay which is very important since it provides information about the cell growth and the metabolic activity of the cells. It might be noticed (Fig. 11) that the levels of MTT conversion increase with time, showing an increasing number of viable cells as a result of the active cell proliferation over the 7 day incubation period. Further, the optical density values were higher in the case of N-implanted alloy with a more significant statistical difference at 4 and 7 days after cell plating. This finding indicates a better osteoblast response to N-implanted Ti-25Ta-25Nb.

The above results are consistent with studies performed by Chien et al. [58] on cell compatibility of TiN and TiAlN films prepared by a reactive radio frequency (RF) magnetron sputter deposition system on nickel-based alloys showing that cell viability and proliferation increased in comparison with the corresponding uncoated surfaces. Since surface topography was almost identical (data not shown) for both surfaces, the differences observed in the cell morphology and proliferation must be a consequence of the chemical composition or wettability or a synergistic effect of both. Thus, we noticed that besides changing surface composition, Hardion+ implantation technique slightly increased the surface wettability of Ti-25Ta-25Nb. The water contact angles of non-treated and N-implanted alloy, measured with a CAM 100 equipment, ranged from $73.514^0 \pm 2.653^0$ to $66.270^0 \pm 1.442^0$. Consequently, N-implantation method makes the surfaces slightly more hydrophilic. The most general rule connecting material properties with cell-substrate compatibility is that anchorage-dependent mammalian cells prefer surfaces with moderate hydrophilicity (water contact angle around 60 degrees) [59]. This finding could explain the potential of N-implanted Ti-25Ta-25Nb to increase osteoblast proliferation in comparison with the non-treated sample.

Taking into consideration that cell-material interaction is a complex and dynamic bi-directional process mimicking to some extent the natural interactions of cells with ECM, namely the cells sense and accept information from cues in the ECM and, at their turn, they produce and frequently remodel their microenvironment [60,61], the next objective of our study has been to evaluate synthesis, secretion and formation of the FN matrix by immunofluorescence. FN is an abundant component of the ECM being adsorbed to this,

together with other adhesion molecules, from either serum within cell culture media, or body fluid within the *in vivo* environment. Cells tend to adhere and rearrange adsorbed ECM proteins on the material surface in a fibril-like pattern. Afterwards, the ECM undergoes proteolytic degradation, a mechanism for the removal of the excess ECM, and attached cells begin to synthesize and secrete their own insoluble matrix [62]. As shown in Fig. 12, at 2 days after cell seeding, the fluorescent staining for FN was detected mainly intracellularly and, to a lesser extent, surrounding the cells. At 7 days post-seeding, FN fibrils were presented in the subcellular area, immediately surrounding the cell periphery and between the cells. These results demonstrate that hFOB 1.19 cells grown in contact with both non-treated and N-implanted Ti-25Ta-25Nb are able to synthesize, secrete and deposit an abundant FN matrix organized into fibrillar networks.

4. Conclusion

In this study, nitrogen implantation performed on a Ni-free superelastic Ti-based alloy was carried out for the first time. It was shown in this study that nitrogen ion implantation performed by the *Hardion+* technology on the Ti-25Ta-25Nb alloy composition strongly modify the superficial properties due to the formation of a titanium-based nitride, which was clearly identified by GIXRD, XPS and SIMS analyses.

A hardness increase was detected in the first 600 nm and a maximum hardness value at about 8.5 GPa is then obtained after N-implantation, which corresponds to an increasing of almost twice the hardness value of the bulk alloy. On the other hand, the N-implantation advantageously modified the wear property reducing the friction coefficient by a factor of 2.7 and the wear track by 85% after 200 cycles under a 0.25N load.

Lower corrosion and ion release rate for the N-implanted surface than for the non-implanted one was determined, demonstrating the beneficial effects of the implantation. Long term monitoring of the open circuit potentials proved a nobler behaviour of N-implanted Ti-25Ta-25Nb alloy due to the barrier properties of the nitride layer.

In vitro tests performed on human fetal osteoblasts indicated that both non-treated and N-implanted Ti-25Ta-25Nb alloy exhibited good level of cytocompatibility. Furthermore, our data show that the tested N-implanted surface can play an active role in tissue biocompatibility resulting in an enhancement of biological properties.

Consequently, this work shows that the N-implanted superelastic Ti-based alloy is very useful for biomedical applications due to the observed better corrosion resistance, excellent biocompatibility and desirable mechanical properties combining the bulk superelastic property and the hard and wear resistant surface. These properties are particularly appreciated for various medical devices such as cardiovascular stents, dental implants, orthodontic arcs, neurologic clips, endodontic drills, orthopaedic prosthesis.

Acknowledgements

This research was funded in the frame of a Eurêka/MNT ERA-Net European consortium, Project "NanoBioAll" Advanced Metallic Biomaterials, Nano-Structured, for Implantable Medical Devices. The authors wish to thank Dr. Simona Popescu (Faculty of Applied Chemistry and Materials Science, University Politehnica of Bucharest) for kind help in measuring the water contact angle.

References

[1] M. Long, H.J. Rack, Titanium alloys in total joint replacement, A materials science perspective. Biomaterials 19 (1998) 1621–1639.

[2] M. Geetha, A.K. Singh, R. Asokamani, A.K. Gogia, Ti based biomaterials, the ultimate choice for orthopaedic implants - A review, Prog. Mater. Sci. 54 (2009) 397–425.

[3] M. Niinomi, Fatigue performance and cyto-toxicity of low rigidity titanium alloy, Ti-29Nb-13Ta-4.6Zr, Biomaterials 24 (2003) 2673–2683.

[4] S.J. Li, T.C. Cui, Y.L. Hao, R. Yang, Fatigue properties of a metastable beta-type titanium alloy with reversible phase transformation, Acta Biomater. 4 (2008) 305–317.

[5] M. Besse, P. Castany, T. Gloriant, Mechanisms of deformation in gum metal TNTZ-O and TNTZ titanium alloys: A comparative study on the oxygen influence, Acta Mater. 59 (2011) 5982–5988.

[6] P. Laheurte, F. Prima, A. Eberhardt, T. Gloriant, M. Wary, E. Patoor, Mechanical properties of low modulus beta titanium alloys designed from the electronic approach, J. Mech. Behav. Biomed. Mater.3 (2010) 565–573.

[7] Y. Al-Zain, H.Y. Kim, H. Hosoda, T.H. Nam, S. Miyazaki, Shape memory properties of Ti-Nb-Mo biomedical alloys, Acta Mater.58 (2010) 4212–4223.

[8] H.Y. Kim, Y. Ikehara, J.I. Kim, H. Hosoda, S. Miyazaki, Martensitic transformation, shape memory effect and superelasticity of Ti-Nb binary alloys, Acta Mater. 54 (2006) 2419–2429.

[9] E. Eisenbarth, D. Velten, M. Müller, R. Thull, J. Breme, Biocompatibility of beta-stabilizing elements of titanium alloys, Biomaterials 25 (2004) 5705–5713.

[10] A. Dobromyslov, G. Dolgikh, Y. Dutkiewicz, T. Trenogina, Phase and structural transformations in Ti-Ta alloys, Phys. Met. Metallogr. 107 (2009) 502–510.

[11] M. Niinomi, M. Nakai, J. Hieda, Development of new metallic alloys for biomedical applications, Acta Biomater. 8 (2012) 3888–3903.

[12] R. Huiskes, H. Weinans, B. Vanrietbergen, The relationship between stress shielding and bone-resorption around total hip stems and the effects of flexible materials, Clin. Orthop. Relat. Res. 124 (1992) 124–134.

[13] M. Niinomi, Mechanical biocompatibilities of titanium alloys for biomedical applications, J. Mech. Behav. Biomed. Mater. 1 (2008) 30–42.

[14] A.Shenhar, I. Gotman, E.Y. Gutmanas, P. Ducheyne, Surface modification of titanium alloy orthopaedic implants via novel PIRAC nitriding method, Mater. Sci. Eng. A 268 (1999) 40–46.

[15] R. Singh, S.G. Chowdhury, S.K. Tiwari, N.B. Dahotre, Laser surface processing of Ti6Al4V in gaseous nitrogen: Corrosion performance in physiological solution, J. Mater. Sci.: Mater. Med. 19 (2008) 1363–1369.

[16] R. Venugopalan, J.J. Weimer, M.A. George, L.C. Lucas, The effect of nitrogen diffusion hardening on the surface chemistry and scratch resistance of Ti-6Al-4V alloy, Biomaterials 21 (2000) 166–177.

[17] F. Yildiz, A.F. Yetim, A. Alsaran, A. Celik, Plasma nitriding behavior of Ti6Al4V orthopedic alloy, Surf. Coat. Technol. 201 (2008) 2471–2476.

[18] X.Y. Liu, P.K. Chu, C.X. Ding, Surface modification of titanium, titanium alloys, and related materials for biomedical applications, Mater. Sci. Eng. R 47 (2004) 49–121.

[19] M.V. Popa, I. Demetrescu, E. Vasilescu, P. Drob, A. Santana-Lopez, J. Mirza-Rosca, C. Vasilescu, D. Ionita, Corrosion susceptibility of implant materials Ti-5Al-4V and Ti-6Al-4Fe in artificial extra-cellular fluids, Electrochim. Acta 49 (2004) 2113–2119.

[20] E Vasilescu,P. Drob, D.Raducanu, V.D. Cojocaru, I. Cinca, D. Iordachescu, R.Ion, M. Popa, C.Vasilescu, In vitro biocompatibility and corrosion resistance of a new implant titanium base alloy, J. Mater. Sci.: Mater. Med. 21 (2010) 1959–1968.

[21] E. Vasilescu, P. Drob, C. Vasilescu, S.I. Drob, E. Bertrand, D.M. Gordin, T. Gloriant, Corrosion resistance of the new Ti-25Ta-25Nb alloy in severe functional conditions, Mater. Corros. 61 (2010) 947–954.

[22] K. Miura, N. Yamada, S. Hanada, T.K. Jung, E. Itoi, The bone tissue compatibility of a new Ti-Nb-Sn alloy with a low Young's modulus, Acta Biomater. 7 (2011) 2320–2326.

[23] D. Mareci, R. Chelariu, D.M. Gordin, G. Ungureanu, T. Gloriant, Comparative corrosion study of Ti-Ta alloys for dental applications, Acta Biomater. 5 (2009) 3625–3629.

[24] V. Barranco, M.L. Escudero, M.C. Garcia-Alonso, Influence of the microstructure and topography and the barrier properties of oxide scales generated on blasted Ti6Al4V surfaces, Acta Biomater. 7 (2011) 2716–2725.

[25] J.J. Ramsden, D.M. Allen, D.J. Stephenson, J.R. Alcock, G.N. Peggs, G. Fuller, G. Goch, The design and manufacture of biomedical surfaces, CIRP Annals – Manufact. Technol. 56 (2007) 687–711.

[26] B. Rauschenbach, Mechanical properties of nitrogen ion-implanted Ti-6Al-4V alloy, Surf. Coat. Technol. 66 (1994) 279–282.

[27] M. Guemmaz, A. Mosser, L. Boudoukha, J.J. Grob, D. Raiser, J.C. Sens, Ion beam synthesis of non-stoichiometric titanium carbide: composition structure and nanoindentation studies, Nucl. Instrum. Meth. Phys. Res. B 111 (1996) 263–270.

[28] R.A. Buchanan, E.D. Jr Rigney, J.M. Williams, Ion implantation of surgical Ti-6Al-4V for improved resistance to wear-accelerated corrosion, J. Biomed. Mater. Res. 21 (1987) 355–366.

[29] C. Johansson, J. Lausmaa, T. Rostlund, P. Thomsen, Commercially pure titanium and Ti6Al4V implants with and without hydrogen-ion implantation: surface characterization and quantitative studies in rabbit cortical bone, J. Mater. Sci.: Mater. Med. 4 (1993) 132–141.

[30] T. Rostlund, P. Thomsen, L.M. Bjursten, L.E. Ericson, Difference in tissue response to nitrogen-ion-implanted titanium and c.p. titanium in the abdominal wall of the rat, J. Biomed. Mater. Res. 24 (1990) 847–860.

[31] H.H. Huang, C.H. Hsu, S.J. Pan, J.L. He, C.C. Chen, T.L. Lee, Corrosion and cell adhesion behavior of TiN-coated and ion-nitrided titanium for dental applications, Appl. Surf. Sci. 244 (2005) 252–256.

[32] E. Bertrand, T. Gloriant, D.M. Gordin, E. Vasilescu, P. Drob, C. Vasilescu, S.I. Drob, Synthesis and characterisation of a new superelastic Ti-25Ta-25Nb biomedical alloy, J. Mech. Behav. Biomed. Mater. 3 (2010) 559–564.

[33] E. Bertrand, P. Castany, T. Gloriant, Investigation of the martensitic transformation and the damping behavior of a superelastic Ti-Ta-Nb alloy, Acta Mater. 61 (2013) 511–518.

[34] J.F. Ziegler, Ion implantation physics, in: J.F. Ziegler (Eds), Handbook of ion implantation technology, Elsevier, Amsterdam, 1992, pp. 1–68.

[35] Z. Cai, H. Nakajima, M. Woldu, A. Berglund, M. Bergman, T. Okabe, In vitro corrosion resistance of titanium made using different fabrication methods, Biomaterials 20 (1999) 183-190.

[36] R. Van Noort, The implant material of today, J. Mater. Sci. 22 (1987) 3801-3811.

[37] S.Y. Yu, J.R. Scully, Corrosion and passivity of Ti-13%Nb-13%Zr in comparison to other biomedical implant alloys, Corrosion 53 (1997) 965-976.

[38] E. Vasilescu, P. Drob, D. Raducanu, I. Cinca, D. Mareci, J.M. Calderon Moreno, M. Popa, C. Vasilescu, J.C. Mirza Rosca, Effect of thermo-mechanical processing on the corrosion resistance of Ti6Al4V alloys in biofluids, Corros. Sci. 51 (2009) 2885-2896.

[39] S.A. Harris, R.J. Enger, B.L. Riggs, T.C. Spelsberg, Development and characterization of a conditionally immortalized human fetal osteoblastic cell-line, J. Bone Miner. Res. 10 (1995) 178–186.

[40] A. Cimpean, S. Popescu, C.M. Ciofrangeanu, A.N. Gleizes, Effects of LP-MOCVD prepared TiO2 thin films on the in vitro behavior of gingival fibroblasts, Mat. Chem. Phys. 125 (2011) 485–492.

[41] T. Mosman, Rapid colorimetric assay for cellular growth and survival: Application to proliferation and cytotoxicity assays, J. Immunol. Methods 65 (1983) 55–63.

[42] I. Milošev, H.H. Strehblow, B. Navinšek, M. Metikoš-Huković, Electrochemical and thermal oxidation of TiN coatings studied by XPS, Surf. Inter. Anal. 23 (1995) 529–539.

[43] J.A. Wilks, N.P. Magtoto, J.A. Kelber, V. Arunachalam, Interfacial reactions during sputter deposition of Ta and TaN films on organosilicate glass: XPS and TEM results, Appl. Surf. Sci. 253 (2007) 6176-6184.

[44] R. Fix, R.G. Gordon, D.M. Hoffman, Chemical Vapor deposition of vanadium, niobium and tantalum nitride thin-films, Chem. Mater. 5 (1993) 614–619.

[45] V. Maurice, G. Despert, S. Zanna, P. Josso, M.P. Bacos, P. Marcus, XPS study of the initial stages of oxidation of alpha(2)-Ti3Al and gamma-TiAl intermetallic alloys, Acta Mater. 55 (2007) 3315–3325.

[46] S. Faghihi, F. Azari, J.A. Szpunar, H. Vali, M. Tabrizian, Titanium crystal orientation as a tool for the improved and regulated cell attachment, J. Biomed. Mater. Res. 91A (2009) 656–662.

[47] S. Samuel, S. Nag, S. Nasrazadani, V. Ukirde, M.E. Bouanani, A. Mohandas, K. Nguyen, R. Banerjee, Corrosion resistance and in vitro response of laser-deposited Ti-Nb-Zr-Ta alloys for orthopedic implant applications, J. Biomed. Mater. Res. 94A (2010) 1251–1256.

[48] G. Jouve, C. Séverac, S. Cantacuzène, XPS study of NbN and (NbTi)N superconducting coatings, Thin Solid Films 287 (1996) 146–153.

[49] D.D. Sarma, C.N.R. Rao, XPES Studies of oxides of 2nd-row and 3rd-row transition metals including rare-earths, J. Elect. Spec. Rel. Phen. 20 (1980) 25–45.

[50] G.R. Gruzalski, D.M. Zehner, Defect states in substoichiometric tantalum carbide, Phys. Rev. B. 34 (1986) 3841–3848.

[51] D.J. Blackwood, A.W.C. Chua, K.H.W. Seah, R. Thampuran, S.H. Teoh, Corrosion behaviour of porous titanium-graphite composite designed for surgical implants, Corros. Sci. 42 (2000) 481–503.

[52] J. Black, Biological performance of materials: Fundamentals of biocompatibility, Marcel Decker Inc, New York, 1992.

[53] E, Blasco-Tamarit, A. Igual-Munoz, J. Garcia-Anton, D.M. Garcia-Garcia, Galvanic corrosion of titanium coupled to welded titanium in LiBr solutions at different temperatures, Corros. Sci. 51 (2009) 1095–2102.

[54] G. Sheela, M. Ramasamy, C.R.K. Rao, M. Pushpavanam, Electrochemical assessment on corrosion behavior of electrochemically joined dissimilar metal joins, Bull. Electrochem. 17 (2001) 347–350.

[55] A. Cimpean, V. Mitran, C.M. Ciofrangeanu, B. Galateanu, E. Bertrand, D.M. Gordin, D. Iordachescu, T. Gloriant, Osteoblast cell behavior on the new beta-type Ti-25Ta-25Nb alloy, Mater. Sci. Eng. C 32 (2012) 1554–1563.

[56] C.Y. Yang, L.Y. Huang, T.L. Shen, J.A. Yeh, Cell adhesion, morphology and biochemistry on nanotopographic oxidized silicon surfaces, Eur. Cell. Mater. 20 (2010) 415-430.

[57] A. Okumura, M. Goto, M. Yoshinari, S. Masuko, T. Katsuki, T. Tanaka, Substrate affects the initial attachment and subsequent behavior of human osteoblastic cells, Biomaterials 22 (2001) 2263–2271.

[58] C.C. Chien, K.T. Liu, J.G. Duh, K.W. Chang, K.H. Chung, Effect of nitride film coatings on cell compatibility, Dent. Mater. 24 (2008) 986–993.

[59] K. Webb, V. Hlady, P.A. Tresco, Relative importance of surface wettability and charged functional groups on NIH 3T3 fibroblast attachment, spreading, and cytoskeletal organization, J. Biomed. Mater. Res. 41 (1998) 422–430.

[60] M. Jayaraman, U. Meyer, M. Buhner, U. Joos, H.P. Wiesmann, Influence of titanium surfaces on attachment of osteoblast-like cells in vitro, Biomaterials 25 (2004) 625–631.

[61] R.O. Hynes, Integrins: Bidirectional, allosteric signaling machines, Cell 110 (2002) 673–687.

[62] V. Llopis-Hernandez, P. Rico, J. Ballester-Beltran, D. Moratal, M. Salmeron-Sanchez, Role of surface chemistry in protein remodeling at the cell-material interface, PLoS ONE 2011;doi:10.1371/journal.pone.0019610.

Figure and table captions

Fig. 1. Stress-strain tensile curve of the superelastic Ti-25Ta-25Nb alloy (from [33]).

Fig. 2. GIXRD patterns of non-treated and N-implanted Ti-25Ta-25Nb alloy.

Fig. 3. XPS depth profiles of N 1s, Ti 2p, Nb 3p and Ta 4d excitation states at a N-implanted Ti-25Ta-25Nb alloy.

Fig. 4. Negative ion depth profiles on a N-implanted Ti-25Ta-25Nb alloy, including a sketch of multi charged ion induced depth profile development on TaN^-.

Fig. 5. Hardness profiles of non-treated and N-implanted Ti-25Ta-25Nb alloy.

Fig. 6. Friction coefficient of non-treated and N-implanted Ti-25Ta-25Nb alloy, as a function of the number of cycles and optical micrographs showing the wear tracks after 200 cycles under 0.25N.

Fig. 7. Cyclic potentiodynamic curves of Ti-25Ta-25Nb alloy in SBF at 37^0C.

Fig. 8. Monitoring of open circuit potentials for Ti-25Ta-25Nb alloy in SBF at 37^0C.

Fig. 9. Comparative evaluation of LDH activity expressed in culture media by hFOB 1.19 cells grown on non-treated and N-implanted Ti-25Ta-25Nb.

Fig. 10. Fluorescence micrographs of hFOB 1.19 cells grown on non-treated and N-implanted Ti-25Ta-25Nb surfaces. Staining with phalloidin-TRITC to detect F-actin filaments (red) and DAPI to label the nuclei (blue).

Fig. 11. Representative data of MTT cell proliferation assay. Formazan absorbance (OD 550 nm) was expressed as a measure of cell proliferation at different time points over the 7-day incubation period. Results are presented as means ±SD (n = 3). *$p < 0.01$ *vs.* hFOB 1.19 cells

grown on non-treated Ti-25Ta-25Nb; **p < 0.001 *vs.* hFOB 1.19 cells grown on non-treated Ti-25Ta-25Nb.

Fig. 12. Fluorescence micrographs showing the immunoreactivity of fibronectin synthesized, secreted and organized into an extracellular fibrillar network by hFOB 1.19 cells grown on non-treated and N-implanted Ti-25Ta-25Nb.

Table 1. Main electrochemical parameters of Ti-25Ta-25Nb alloy after 2000 immersion hours in SBF at 37^0C

Table 2. Corrosion and ion release rates of Ti-25Ta-25Nb alloy after 2000 immersion hours in SBF at 37^0C

Table 3. Monitoring of the open circuit potential gradients of Ti-25Ta-25Nb alloy for 2000 immersion hours in SBF at 37^0C

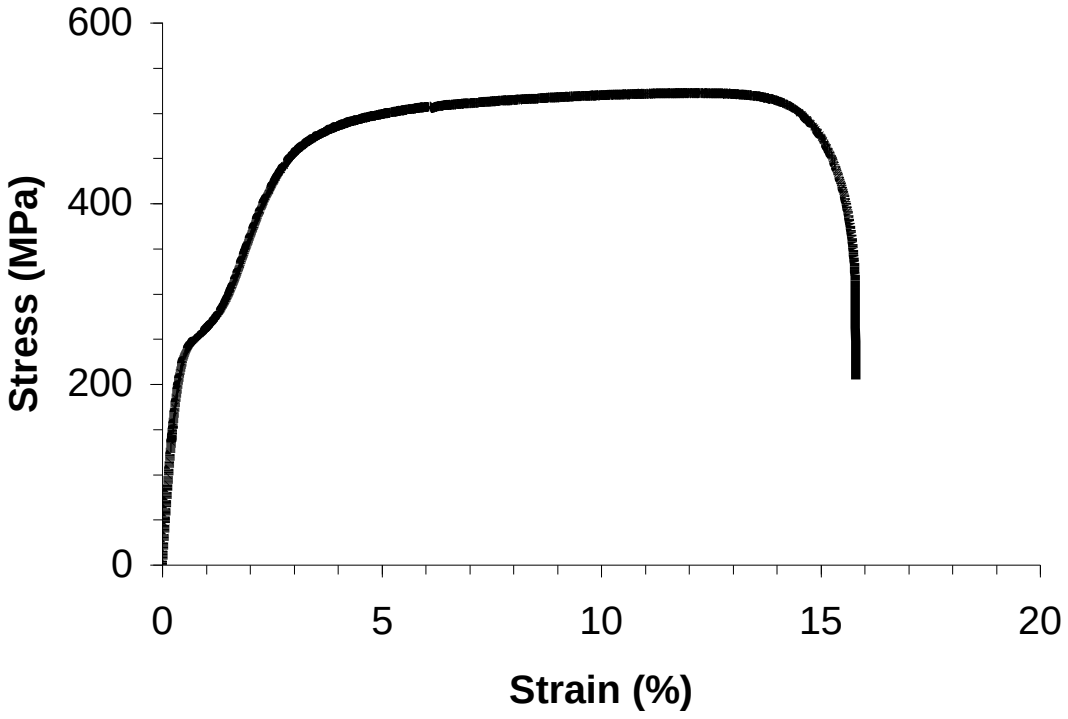

Fig. 1

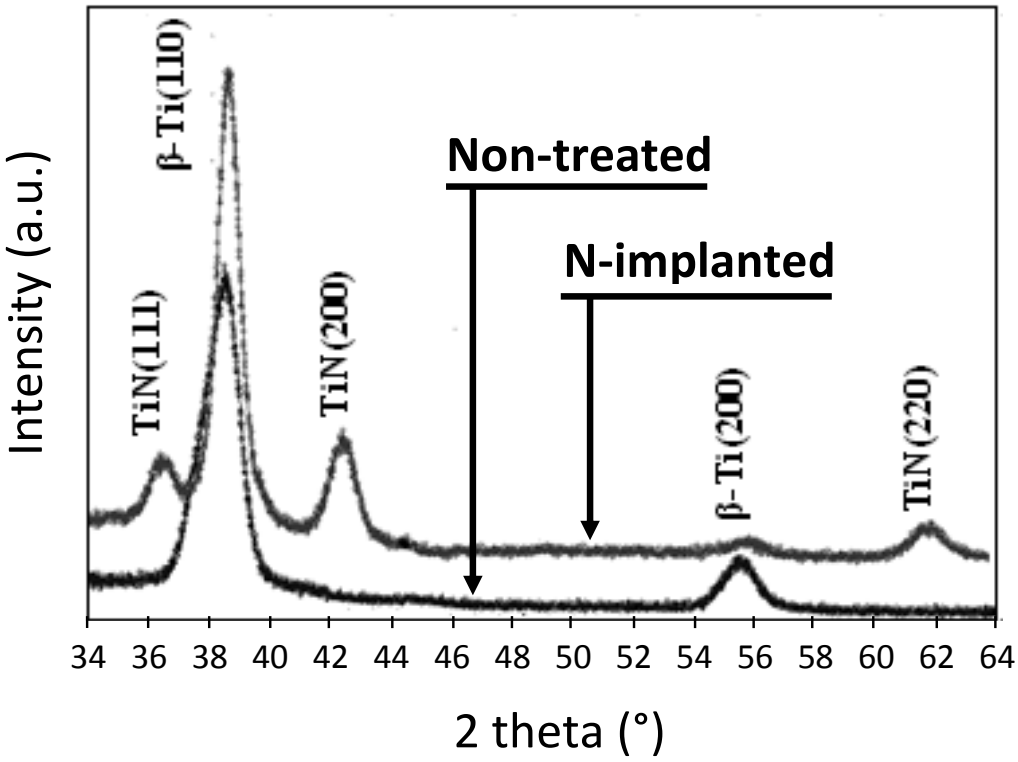
Intensity (a.u.)
β-Ti(110)
TiN(111)
TiN(200)
Non-treated
N-implanted
β-Ti(200)
TiN(220)
34 36 38 40 42 44 46 48 50 52 54 56 58 60 62 64
2 theta (°)

Fig.2

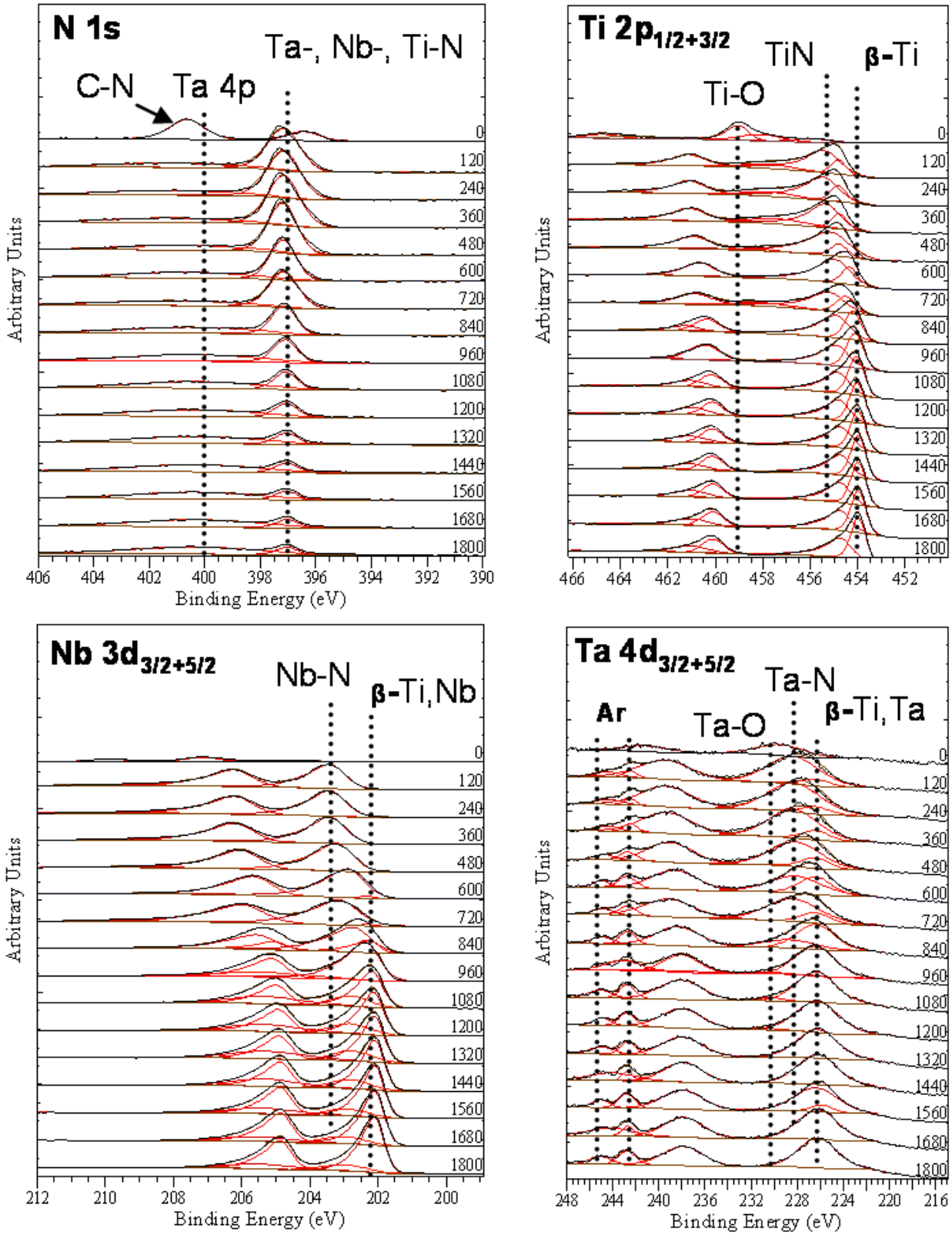
N 1s
Ta-, Nb-, Ti-N
C-N
Ta 4p
Arbitrary Units
Binding Energy (eV)
Ti 2p1/2+3/2
TiN
β-Ti
Ti-O
Nb 3d3/2+5/2
Nb-N
β-Ti,Nb
Ta 4d3/2+5/2
Ta-N
Ar
Ta-O
β-Ti,Ta

Fig.3

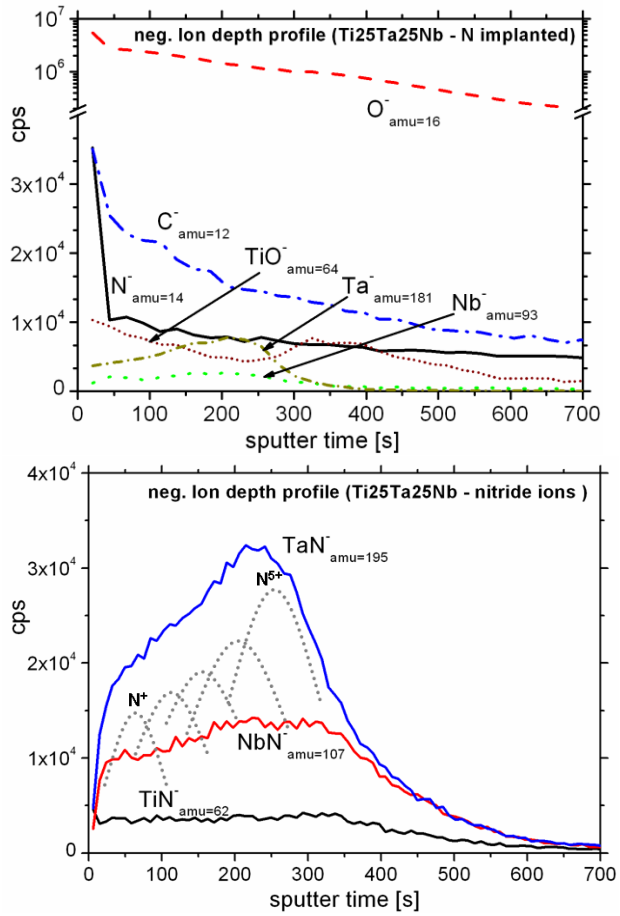
neg. Ion depth profile (Ti25Ta25Nb - N implanted)
cps
sputter time [s]
O- amu=16
C- amu=12
TiO- amu=64
N- amu=14
Ta- amu=181
Nb- amu=93
neg. Ion depth profile (Ti25Ta25Nb - nitride ions)
TaN- amu=195
N5+
N+
NbN- amu=107
TiN- amu=62

Fig.4

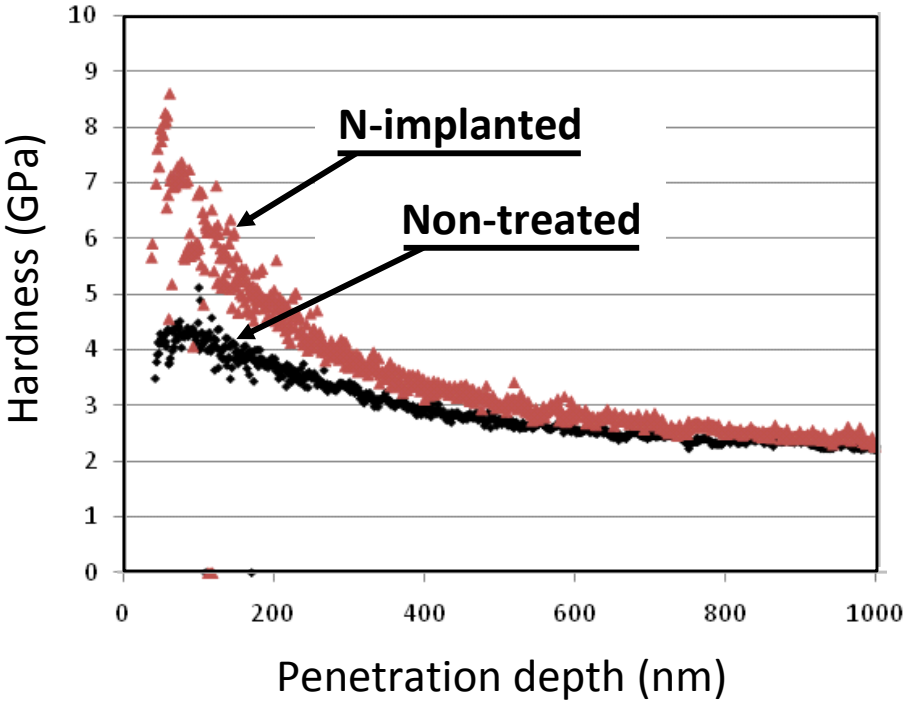
Hardness (GPa)
10
9
8
7
6
5
4
3
2
1
0
N-implanted
Non-treated
0
200
400
600
800
1000
Penetration depth (nm)

Fig.5

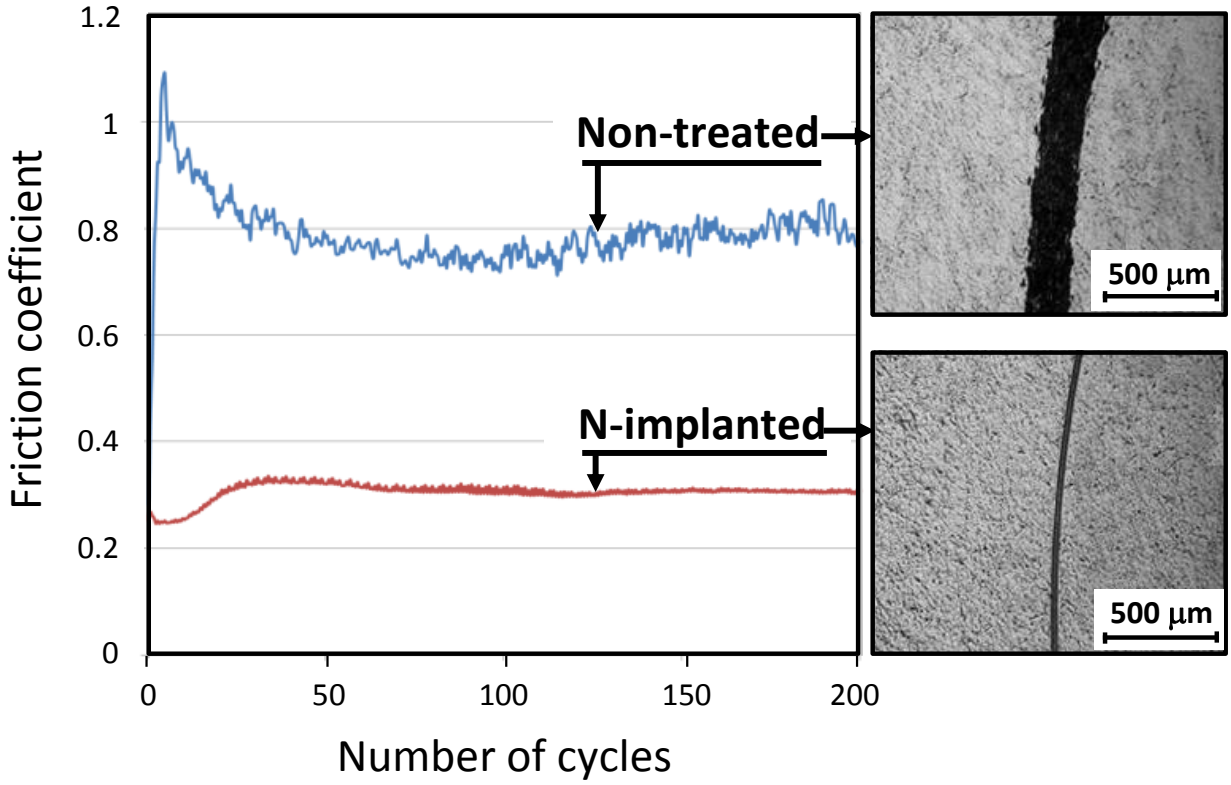
Friction coefficient
1.2
1
0.8
0.6
0.4
0.2
0
0
50
100
150
200
Number of cycles
Non-treated
N-implanted
500 µm
500 µm

Fig.6

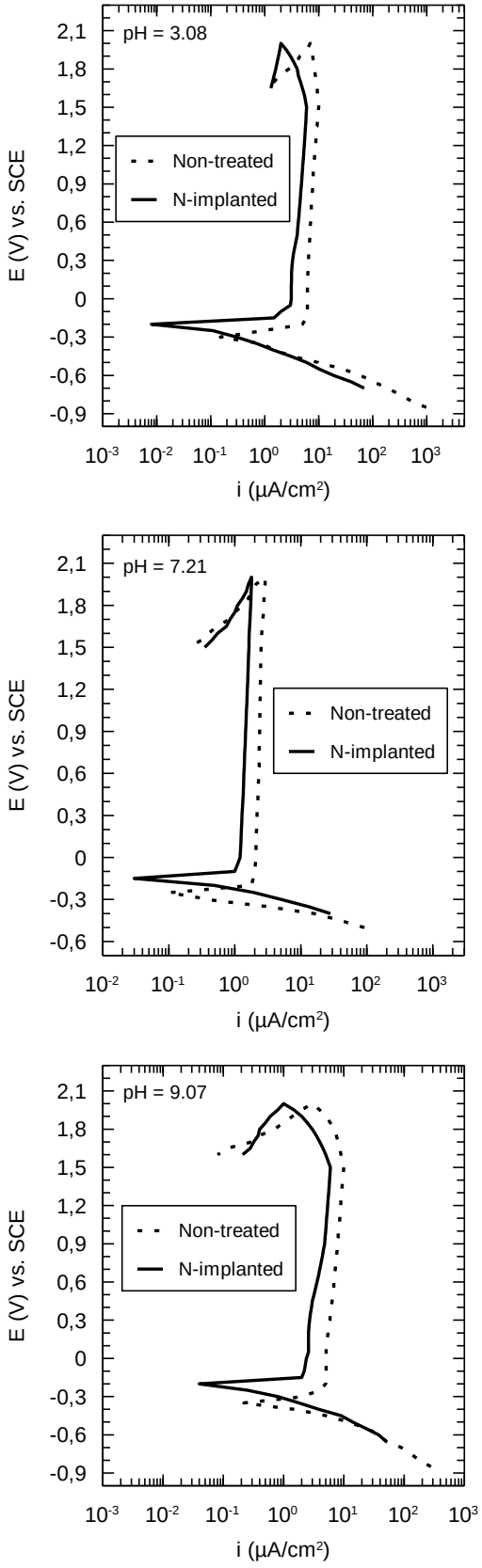
pH = 3.08
Non-treated
N-implanted
E (V) vs. SCE
2,1
1,8
1,5
1,2
0,9
0,6
0,3
0
-0,3
-0,6
-0,9
10-3 10-2 10-1 100 101 102 103
i (µA/cm2)
pH = 7.21
Non-treated
N-implanted
E (V) vs. SCE
2,1
1,8
1,5
1,2
0,9
0,6
0,3
0
-0,3
-0,6
10-2 10-1 100 101 102 103
i (µA/cm2)
pH = 9.07
Non-treated
N-implanted
E (V) vs. SCE
2,1
1,8
1,5
1,2
0,9
0,6
0,3
0
-0,3
-0,6
-0,9
10-3 10-2 10-1 100 101 102 103
i (µA/cm2)

Fig. 7

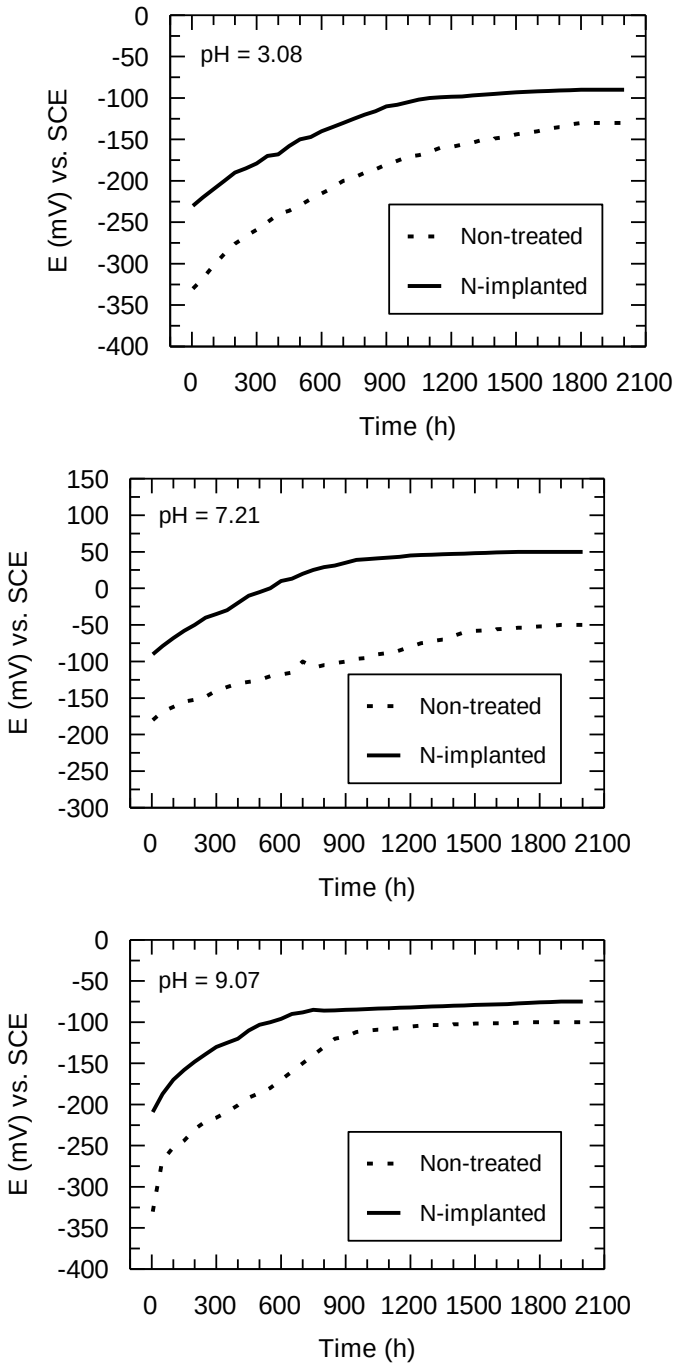
pH = 3.08
E (mV) vs. SCE
Time (h)
Non-treated
N-implanted
pH = 7.21
E (mV) vs. SCE
Time (h)
Non-treated
N-implanted
pH = 9.07
E (mV) vs. SCE
Time (h)
Non-treated
N-implanted

Fig. 8

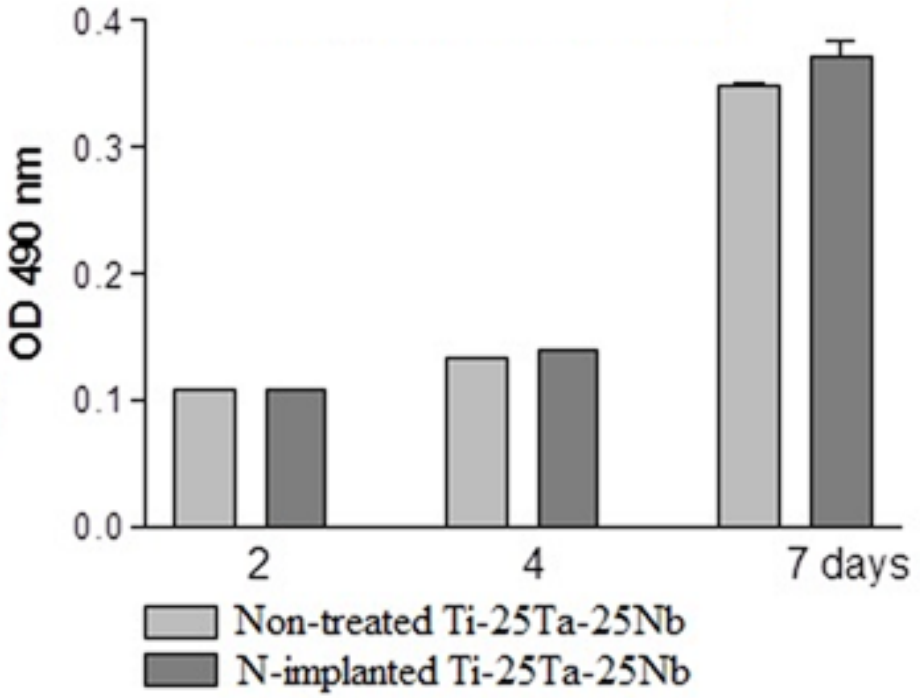
OD 490 nm
0.4
0.3
0.2
0.1
0.0
2
4
7 days
Non-treated Ti-25Ta-25Nb
N-implanted Ti-25Ta-25Nb

Fig. 9

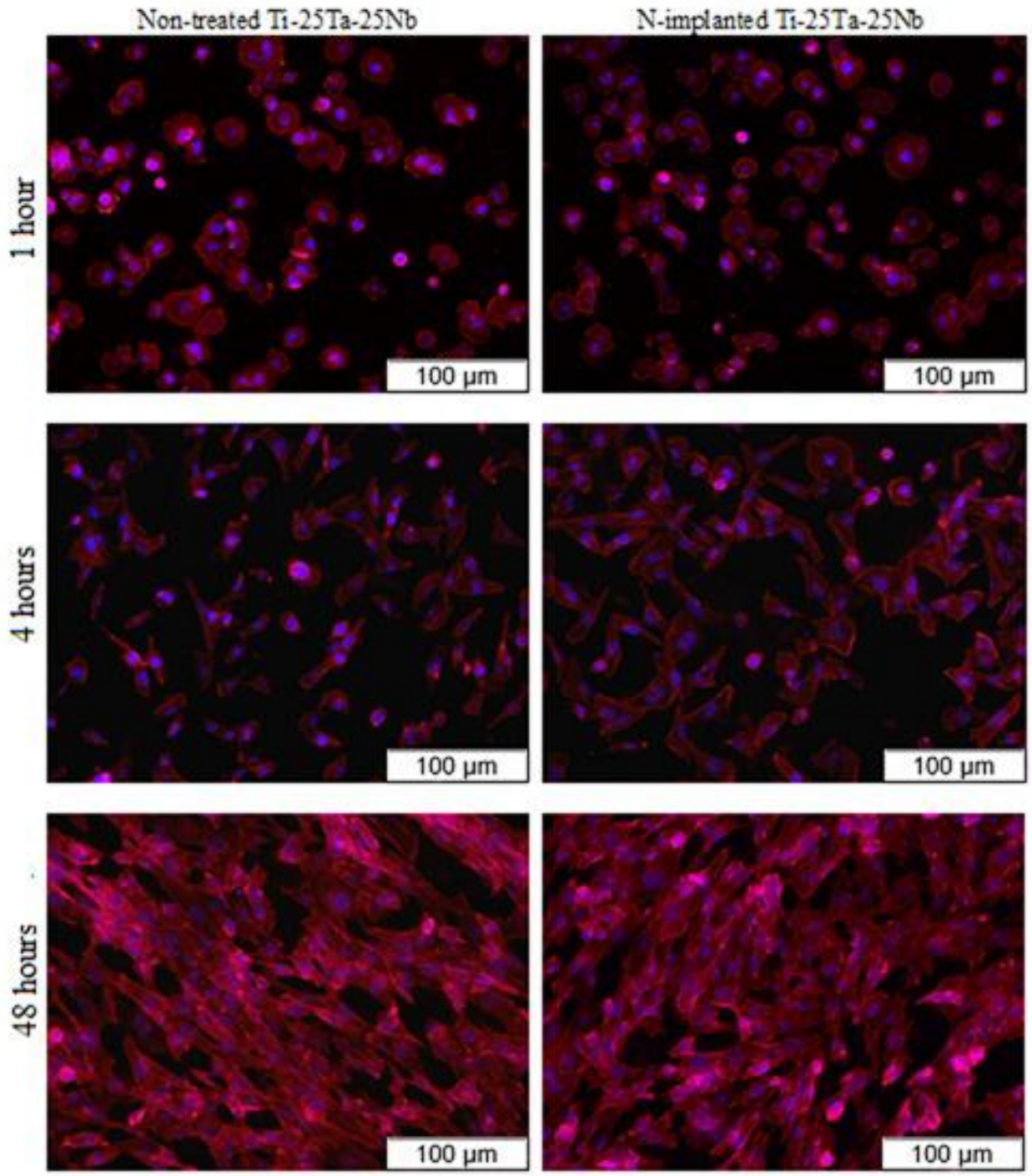
Non-treated Ti-25Ta-25Nb
N-implanted Ti-25Ta-25Nb
1 hour
4 hours
48 hours
100 µm
100 µm
100 µm
100 µm
100 µm
100 µm

Fig. 10

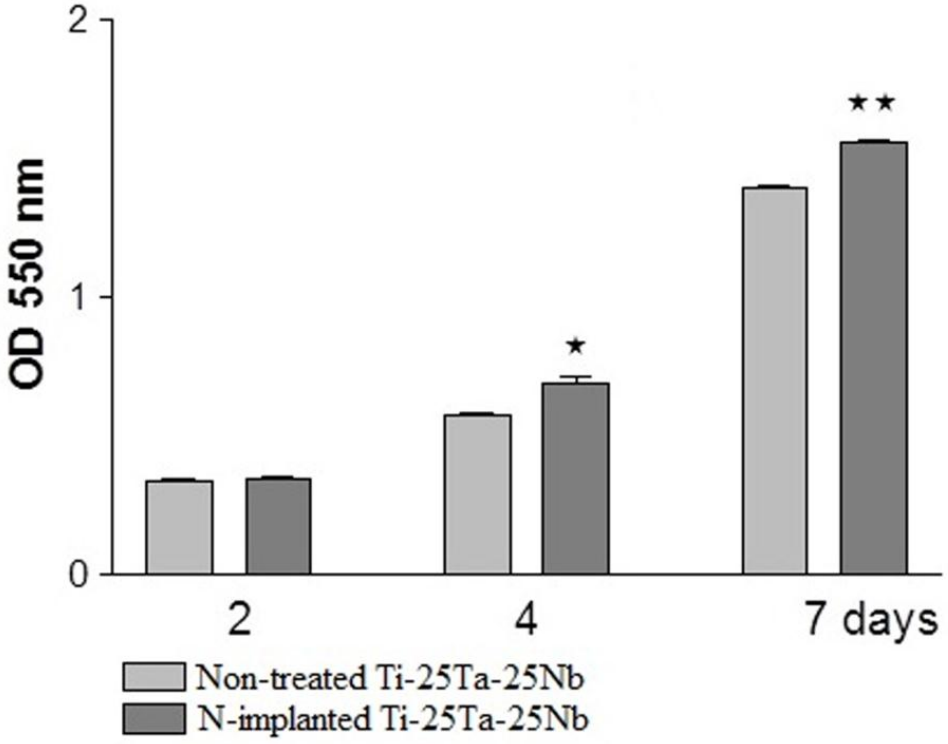
OD 550 nm
2
1
0
★
★★
2
4
7 days
Non-treated Ti-25Ta-25Nb
N-implanted Ti-25Ta-25Nb

Fig. 11

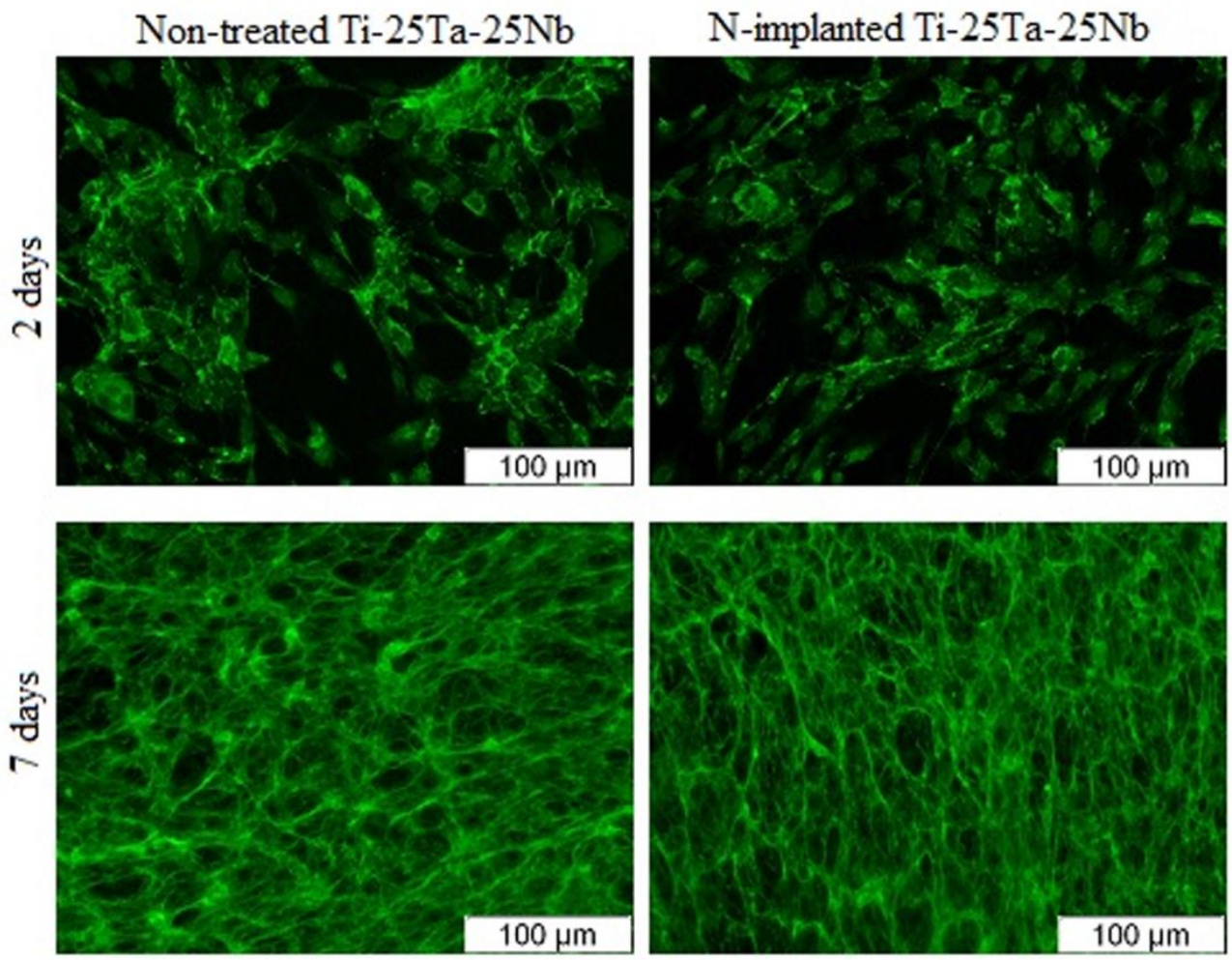
Non-treated Ti-25Ta-25Nb
N-implanted Ti-25Ta-25Nb
2 days
7 days
100 µm
100 µm
100 µm
100 µm

Fig. 12

Table 1

Alloy	E_{corr} (mV)	E_p (mV)	ΔE_p (mV)	$\lvert E_{corr} - E_p \rvert$ (mV)	i_p ($\mu A\ cm^{-2}$)
pH = 3.08					
Non-treated	-310.3	-260.2	>2000	50.1	6.2
N-implanted	-209.5	-170.2	>2000	39.3	3.1
pH = 7.21					
Non-treated	-251.2	-220.1	>2000	31.1	2.1
N-implanted	-153.5	-130.2	>2000	23.3	1.2
pH = 9.07					
Non-treated	-298.4	-250.1	>2000	48.3	5.1
N-implanted	-201.6	-166.2	>2000	35.4	2.6

Table 2

Alloy	i_{corr} ($\mu A\ cm^{-2}$)	V_{corr} ($\mu m\ Y^{-1}$)	Resistance class	R_p ($k\Omega\ cm^2$)	Ion release ($ng\ cm^{-2}$)
pH = 3.08					
Non-treated	0.0916	0.812	Perfect Stable	975	82.50
N-implanted	0.00735	0.0639	Perfect Stable	1230	6.49
pH = 7.21					
Non-treated	0.0276	0.245	Perfect Stable	1173	24.80
N-implanted	0.00219	0.0194	Perfect Stable	1850	1.98
pH = 9.07					
Non-treated	0.0835	0.745	Perfect Stable	990	75.29
N-implanted	0.00698	0.0619	Perfect Stable	1290	6.29

Table 3

Alloy	Time (h)	ΔE_{oc1} (mV)	ΔE_{oc2} (mV)	ΔE_{oc3} (mV)
Non-treated	24	-150.2	0.5	150.1
	500	-104.1	-43.2	61.3
	1000	-72.9	-61.1	11.4
	1500	-86.3	-43.5	43.2
	2000	-80.6	-30.3	50.5
N-implanted	24	-40.8	-21.4	29.6
	500	-145.5	-47.6	98.7
	1000	-65.9	-21.5	34.9
	1500	-45.3	-14.7	31.8
	2000	-40.2	-15.8	25.2